applied sciences

MDPI

Article

Mesh-Free Analysis of a Vertical Axis Wind Turbine Using Lattice Boltzmann Method and Various Turbulence Models

Cinar Laloglu * and Emre Alpman

Department of Mechanical Engineering, Marmara University, 34722 Istanbul, Turkey; emre.alpman@marmara.edu.tr
* Correspondence: cinar.laloglu@brenpower.com

Abstract: This study aims to investigate the aerodynamic analysis of a Darrieus-type vertical axis wind turbine (VAWT) using the Lattice Boltzmann Method (LBM). The objective is to assess the accuracy and performance of the meshless LBM approach in predicting torque coefficients, velocity, turbulence intensity, and vorticity distributions for VAWT aerodynamic analysis. Two turbulence modelling approaches, Large Eddy Simulation (LES) and Reynolds-Averaged Navier-Stokes (RANS), are employed to model the flow domain. The central problem revolves around comparing the performance of different turbulence models based on their agreement with experimental results for power and torque coefficients. The findings demonstrate the effectiveness of the WALE turbulence model in achieving the best agreement with experimental data. Overall, the study provides valuable insights into applying LBM in VAWT aerodynamic analysis and highlights the advantages of the meshless approach compared to traditional CFD methods.

Keywords: Lattice Boltzmann Method (LBM); turbulence modelling; Large Eddy Simulation (LES); Reynolds-Averaged Navier-Stokes (RANS); meshless approach

check for updates

Citation: Laloglu, C.; Alpman, E. Mesh-Free Analysis of a Vertical Axis Wind Turbine Using Lattice Boltzmann Method and Various Turbulence Models. *Appl. Sci.* **2023**, *13*, 8800. https://doi.org/10.3390/app13158800

Academic Editor: Frede Blaabjerg

Received: 1 July 2023
Revised: 18 July 2023
Accepted: 28 July 2023
Published: 30 July 2023

1. Introduction

Most wind turbines are installed in open rural areas due to their better wind potential. Horizontal axis wind turbines (HAWTs) are the preferred configuration and have become a mature technology for converting wind energy into electricity. However, vertical axis wind turbines (VAWTs) also offer their advantages. One notable advantage is that VAWTs can generate power independently of the wind direction, eliminating the need for a yaw control device. VAWTs can be broadly categorized into two types: Savonius and Darrieus. The straightforward blade design of the Darrieus-type vertical axis wind turbine (VAWT) makes it a popular choice in the small-scale wind turbine market [1]. However, one of the challenges with VAWTs is the impact of wake effects, as the blades periodically pass through the wakes generated by other blades. Accurately predicting and understanding these wake interactions is crucial for analysing VAWT aerodynamics.

One major advantage of VAWTs is their versatility in terms of location. They can be used in various locations within open rural areas. Additionally, VAWTs are often considered standalone systems, allowing the generator to be placed at ground level for easier access and maintenance [1]. It is important to note that wind turbine technology is constantly evolving, and ongoing research and development efforts are focused on improving the efficiency, reliability, and cost-effectiveness of both HAWTs and VAWTs. The choice between HAWTs and VAWTs depends on the specific application, site conditions, and project requirements.

Thanks to advancements in computer technology, we can now perform accurate and detailed flow field simulations using three-dimensional computational fluid dynamics (CFD) analyses. These technologies have enabled a wide range of studies on blade shape development. However, traditional numerical methodologies used in CFD, such as finite volume and finite element methods, still face significant challenges in solving real

industrial problems [2]. This study introduces a novel approach that involves solving the Boltzmann equation, which describes the statistical distribution of particles in a fluid in phase space, instead of using the Navier-Stokes equations that describe the flow of a Newtonian fluid under the continuum assumption. Particle-based approaches offer several advantages in obtaining discrete solutions for flow fields. The lattice Boltzmann method (LBM) is a valuable tool for linking the behaviour of particles at both macroscopic and microscopic scales. It accomplishes this by utilizing microscopic models and mesoscopic kinetic equations. Essentially, LBM constructs simplified kinetic models that encapsulate the essential physics of microscopic phenomena. These models are designed to ensure that the macroscopic properties derived from them conform to the desired macroscopic equations, thereby facilitating a comprehensive understanding of the system under investigation.

Furthermore, LBM allows for reduced computational costs by utilizing a lattice structure. This approach effectively simulates continuum flows, unlike traditional particle-based methods that can produce unstable solutions when the number of particles increases. Additionally, traditional particle-based approaches may have limited accuracy in multi-dimensional flows, and it can be challenging to derive error estimates as the sample points do not have fixed positions. Overall, the application of the Boltzmann equation solved using the lattice Boltzmann method presents a promising alternative to traditional numerical methodologies in CFD, overcoming some of their limitations and providing new insights into flow field simulations.

LBM offers several advantages over traditional CFD methods, particularly in handling complex geometries and boundaries. Researchers have shown that LBM is highly suitable for simulating intricate geometries and complex boundary conditions [3,4]. The flexibility of the lattice-based grid structure in LBM allows for easy representation of irregular geometries and accurate capture of flow features.

Moreover, LBM excels in simulating multi-scale and multiphase flows. Recent studies have demonstrated the capability of LBM in microfluidics applications [5] and multiphase flows with phase change phenomena [6]. The mesoscopic nature of LBM enables accurate modelling of flow behaviour at different length scales, leading to improved accuracy in numerical predictions. Efficient parallelization is another strength of LBM, enabling high-performance computing for large-scale simulations. This is particularly advantageous for turbulent flow simulations and aerodynamic analyses. Researchers have successfully employed LBM in simulating turbulent flows with excellent scalability and computational efficiency [7,8].

Furthermore, LBM provides a natural framework for incorporating complex physics, such as thermal effects and fluid-structure interactions. Recent work has shown the capability of LBM in accurately capturing heat transfer phenomena in porous media [9] and simulating fluid-structure interactions [4]. These advancements in modelling complex physics contribute to more realistic and comprehensive numerical results.

LBM has emerged as a powerful tool for enhancing the quality of numerical results in CFD applications. Its ability to handle complex geometries, simulate multi-scale and multiphase flows, efficient parallelization, and incorporate complex physics makes it a promising choice for researchers.

The emergence of computational fluid dynamics (CFD) solutions using the Lattice Boltzmann method (LBM) has led to advancements in meshingless approaches in CFD simulations [6,10]. While LBM is often referred to as a mesh-free method, it is essential to note that it does utilize lattice structures, such as Cartesian grids, for simulation purposes. Therefore, "meshingless" is more appropriate in describing the method's characteristic of not requiring a body-fitting mesh during CFD solutions. In meshingless CFD simulations, lattice structures are present around the geometry in the flow field, with the size of the lattice depending on the virtual wind tunnel size or flow area for internal/external flow analysis. The resolution of the Cartesian grids is determined by a given value at the resolved scale. Refinement algorithms can control the solution, enabling different methods based on near-static walls and solution adaptivity. This solution-adaptive meshingless

approach is beneficial for addressing challenges related to complex geometries, moving structures in the flow field, and fluid-structure interaction [11,12]. The absence of mesh generation and the capability to solve adaptively make meshingless techniques, especially LBM, increasingly popular in CFD [10]. Traditional CFD methods based on meshing techniques have limitations, as they heavily rely on the quality of the mesh, which can be time-consuming to generate.

Also, handling changes in the domain topology, such as problems involving moving parts or fluid-structure interaction, can be challenging. The LBM overcomes many of these drawbacks and offers a promising alternative, as it is based on a particle-based, fully Lagrangian approach and does not require a mesh for discretization. Commercial CFD software like XFlow (Next Limit Technologies) utilizes LBM to simulate complex problems such as aerodynamics, aero-acoustics, and fluid-structure interaction [13]. The simulation of wake effects in straight-bladed wind turbines presents a challenge due to the shedding and trailing vortices system. Adaptive wake refinement techniques can be employed to capture the wake by refining the lattice structures around the blades in both coarse and fine resolutions, allowing for the investigation of the aerodynamic performance of the blades. XFlow incorporates an adaptive wake refinement feature based on the vorticity field in the lattice elements, triggering automatic refinement when a threshold value is reached [11]. Previous studies have examined the performance of vertical axis wind turbines (VAWTs) using various simulation methods. Ref. [3] compared wind tunnel tests and three-dimensional numerical analysis of a Darrieus VAWT, finding that 2D simulations performed significantly better than 3D simulations, primarily due to large tip vortices in the real turbine. Ref. [14] utilized LBM to simulate a 2D incompressible flow over Savonius VAWTs with different shapes, successfully implementing bounce-back boundary conditions at large lattice sizes to simulate curved boundaries. Experimental measurements and computational simulations have also been employed to understand the flow structures and performance of VAWTs. Ref. [2] used large eddy simulation (LES) with a dynamic Smagorinsky subgrid-scale model to accurately predict the performance of VAWTs with fixed- and variable-pitch mechanisms. Ref. [15] compared CFD solutions using the RNG k-ε turbulence model to experimental data, revealing interesting observations at different tips. In this study, the Lattice-Boltzmann method was applied to solve the flow field around a straight-bladed Darrieus-type 500W VAWT using Reynolds Averaged Navier-Stokes (RANS) and Large-Eddy Simulation (LES) approaches to model the turbulence in the flow field. Spalart-Allmarass one equation turbulence model was selected for the RANS, while Wall-Adapting Local Eddy (WALE) and Smagorinsky sub-grid scale models were used for LES. Predicted power and torque coefficient at three tip speed ratios (TSR) were compared to the experimental data from [15]. CFD solutions with a coarse and fine lattice structure were applied using XFLOW commercial CFD software.

2. Numerical Methodology

2.1. Lattice-Boltzmann Method

The Lattice-Boltzmann method follows a mesoscopic approach wherein the dynamics of fluid particles are approximated by interactions between particles on a regular lattice. The fluid flow is modelled by the collective behaviour of these particles. The Boltzmann equation exists as a single particle distribution function f takes the following form:

$$\frac{\partial f}{\partial t} + \vec{v}.\nabla f = \Omega(f) \tag{1}$$

where $f(\vec{x}, \vec{v}, t)$ related to the probability of encountering particles with the continuous.

The velocity of microscopic particles at a specific position x and time t is denoted by $\vec{c}$, while the collision operator $\Omega(f)$ governs the rate of change in the distribution function f during collisions. In many applications involving the kinetic theory of fluid dynamics, the collision term Ω_i^{BGK} is commonly represented as $\Omega(f)$ using a complex integral formulation. However, to simplify calculations, a widely used approximation

known as the "BGK approximation" was introduced by Bhatnagar, Gross, and Krook. This approximation, integrated by [16], replaces the integral term with a simpler form, as demonstrated in Equation (3).

$$\Omega(f) = \frac{1}{\tau}\left(f_i^{eq} - f_i\right) \tag{2}$$

The collision operator models the collision's effect as the relaxation of the distribution function f towards a steady-state distribution, known as the Maxwellian distribution f_i^{eq}. The parameter τ represents a characteristic time determining the frequency at which the distribution function relaxes towards equilibrium.

To discretize the Boltzmann equation, the continuous velocity space is discretized into a finite set of velocities, denoted as $\vec{V} = \left\{\vec{c}_0, \vec{c}_1, \ldots, \vec{c}_{n-1}\right\}$. Consequently, the distribution function $f(\vec{x}, \vec{v}, t)$ is reduced to $f_i(\vec{x}, t)$, which describes the distribution on a finite lattice.

BGK converted with the Boltzmann equation is simplified to LBGK, which is the discrete Boltzmann equation in [17];

$$\frac{df_i}{dt} + c_i.\nabla f_i = \frac{1}{\tau}\left(f_i^{eq} - f_i\right) \tag{3}$$

The f^{eq} in Equation (3) is the equilibrium distribution function for density. The equation undergoes a discretization process using a spatial step size Δx and a temporal step size Δt, which are related by the following expression: $\frac{\Delta x}{\Delta t} = c_i$. This discretization ensures that the particles in a node x move in time Δt toward a neighbour node $x + c_i\Delta t$ along the vector $\vec{c}_i$ and the equation is [16];

$$f_i(\vec{x} + \vec{c}_i dt, t + dt) - f_i(\vec{x}, t) = \frac{1}{\tau}(f_i^{eq} - f_i(\vec{x}, t)) \tag{4}$$

This method consists of the following two steps:

1. Streaming: During each time step Δt, the particles undergo movement along the lattice bonds to adjacent lattice nodes. The distribution function $f_i{}^*(\vec{x},\ t)$ propagates along the vector $\vec{c}_i$, and at the updated time $t + \Delta t$, the distribution function at a neighbouring $f_i(\vec{x} + \vec{c}_i dt, t + dt) = f_i{}^*(\vec{x},\ t)$
2. Collision: At time t, the particles located at a specific node x interact, leading to changes in their velocity directions. As a result of this collision, the distribution function transitions from $f_i(\vec{x},\ t)$ to $f_i{}^*(\vec{x},\ t) = \frac{1}{\tau}(f_i^{eq} - f_i(\vec{x},\ t))$, where τ is a characteristic time representing the relaxation rate of the distribution function towards its equilibrium state f_i^{eq}.

In the three-dimensional lattice Boltzmann method (LBM), the physical space is discretized into uniform Cartesian cells known as lattices. Each lattice unit consists of nodes interacting with their neighbouring nodes through a set of lattice velocities determined as part of the solution. LBM schemes are categorized based on the spatial dimension (d) and the number of distribution functions (b), denoted as DdQb. The commonly used schemes in two dimensions are D2Q7 and D2Q9, while in three dimensions, schemes such as D3Q13, D3Q15, D3Q19, and D3Q27 are widely employed. The XFlow solver, for instance, utilizes the D3Q27 lattice model, which consists of twenty-seven velocities, as depicted in Figure 1.

By employing these lattice models, the LBM can accurately simulate fluid flow and capture complex flow phenomena in three-dimensional space. Each lattice node carries information about the fluid's local characteristics, such as velocity and density, allowing for the simulation of various fluid dynamics problems.

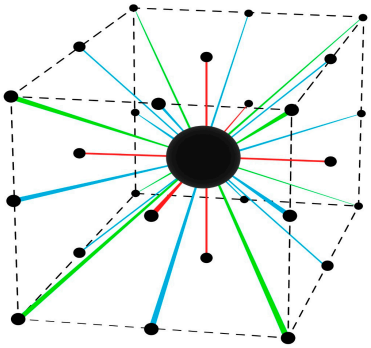

Figure 1. The lattice structure of the D3Q27 model. Each colour shown velocity direction is associated with a lattice node, and the arrangement of these nodes forms a 3D grid.

Usually, the discretized equilibrium distribution function for D3Q27 adopts the following expression [2]:

$$f_i^{eq} = \rho\omega_i(1 + \frac{3}{c_s^2}(e_{ia}u_a) + \frac{9}{2c_s^4}(e_{ia}u_a)^2 - \frac{3}{2c_s^2}(u_a)^2) \quad (5)$$

where e_{ia} discrete velocity, c_s is the sound speed, u the macroscopic velocity, ω_i are built to preserve the isotropy.

For this purpose, the D3Q27 scheme has been implemented for the analysis of VAWT and Wall-Adapting Local Eddy-viscosity (WALE), Spalart-Allmaras and Smagorinsky turbulence models have been selected to analyse static pressure, velocity, and turbulence models. The WALE has good properties both near to and far from the wall turbulent flows [17,18].

2.2. Darrieus VAWT Numerical Model

Vertical axis wind turbines (VAWTs) are commonly categorized into two main types: drag-driven turbines, such as the Savonius design, and lift-driven turbines, like the Darrieus design. While drag-driven turbines tend to have better initial start-up performance, they exhibit lower power generation efficiency than lift-driven turbines. This investigation evaluates the performance of a Darrieus-type wind turbine operating at a wind speed of 12 m/s. The straight blades of the turbine utilize the NACA 0015 airfoil profile. The specific characteristics of the VAWT employed in the virtual wind tunnel simulation conducted by [15] are as follows: the chord length is 150 mm, the rotor diameter (D) is 740 mm, the length (L) is 600 mm, and the aspect ratio (L/D) is 0.81. The turbine consists of three blades. Figure 2 illustrates a schematic CAD representation of the Darrieus VAWT employed in this study, with dimensions matching those of the experimental research conducted by [15]. The Reynolds number for the given air velocity values at 12 m/s is approximately 120,000.

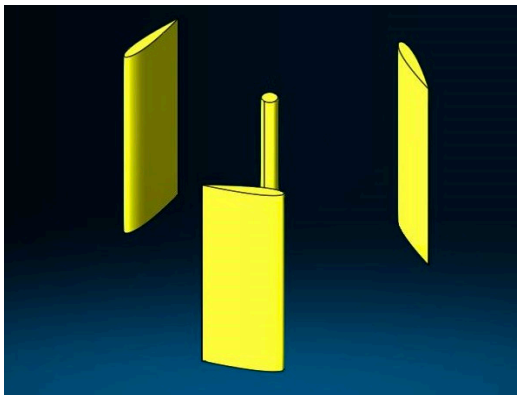

Figure 2. CAD geometry of Darrieus Vertical Axis Wind Turbine.

2.3. Turbulence Models

Selecting a turbulence model is essential to ensure that accurate numerical solutions can be obtained in a reasonable time. Two turbulence modelling approaches were used during the computations: LES and RANS.

2.3.1. Large Eddy Simulation (LES)

In Large Eddy Simulation (LES), an essential aspect is the representation of sub-grid scale stresses. This study employed two different models, namely WALE and Smagorinsky models, to address this task. During LES simulations, turbulent eddy viscosity v_t is introduced as an additional viscosity to capture the characteristics of turbulence. The value of this eddy viscosity is determined by the chosen model [19].

$$v_t = C_x^2 \Delta x^2 \overline{\overline{\omega}} \tag{6}$$

Here, C_x represents a constant specific to the chosen LES model, Δx refers to the spacing between lattice points, and $\overline{\overline{\omega}}$ corresponds to the LES model operator. In the lattice Boltzmann model, the viscosity is connected to the relaxation time τ. This relationship governs the rate at which the distribution function approaches equilibrium. By appropriately adjusting the relaxation time, the desired viscosity can be achieved, influencing the flow behaviour in the simulation.

$$v_{total} = v_o + v_t = \frac{2\tau_o - 1}{6} + \frac{\tau_t}{3} \tag{7}$$

The relaxation time τ can be decomposed into molecular and turbulent components, analogous to the separation of the viscosity term. This allows for distinguishing the contributions of molecular viscosity v_o and turbulent effects. The total relaxation time encompasses both these aspects, as expressed by the following equation:

$$\tau_{total} = 3v_{total} + 0.5 \tag{8}$$

By applying Equation (8), we arrive at:

$$\tau_{total} = 3(v_o + C_x^2 \Delta x^2 \overline{\overline{\omega}} + 0.5) \tag{9}$$

Derived the operator $\overline{\overline{\omega}}$ exclusively from the shear stress tensor for Smagorinsky as follows:

$$\overline{\overline{\omega}} = \sum_{i,j} S_{ij} S_{ij}$$

The WALE model considers the shear stress tensor, including the rotation tensor. The operator $\overline{\overline{\omega}}$ is defined as follows:

$$\overline{\overline{\omega}} = \frac{\left(G_{ij}^d G_{ij}^d\right)^{\frac{3}{2}}}{\left(S_{ij} S_{ij}\right)^{\frac{5}{2}} + \left(G_{ij}^d G_{ij}^d\right)^{\frac{5}{4}}}$$

The difference between WALE and Smagorinsky, LES model constant was given the value of C_x, 0.325 and 0.12, respectively, in Equation (6).

2.3.2. Reynolds-Averaged Navier-Stokes (RANS)

In the context of RANS simulations, the Spalart-Allmaras turbulence model is a one-equation model solving a transport equation for a variable called $\widetilde{v}$, representing an approximation of viscosity [20,21]. This variable is then used to adjust a turbulent viscosity ν_t. Within the lattice Boltzmann method (LBM), the turbulent viscosity can be employed to modify the relaxation time in the collision operator. In this investigation, a modified version of the model, presented in Equation (10), was implemented to enhance

the numerical behaviour near the wall within the laminar sublayer. The transport equation and the complete set of parameters associated with the model are provided below:

$$\frac{\partial \overline{v}}{\partial t} + \vec{u}.\left(\vec{\nabla}\widetilde{v}\right) = \frac{1}{\sigma}\left[\vec{\nabla}.\left((v+\widetilde{v})\vec{\nabla}\widetilde{v}\right) + c_{b2}\left(\vec{\nabla}\widetilde{v}\right)^2\right] + c_{b1}\widetilde{S}\widetilde{v} - c_{w1}f_w\left(\frac{\overline{v}}{d}\right)^2 \quad (10)$$

$$v_t = \widetilde{v}f_{v1}, \quad f_{v1} = \frac{X^3}{X^3 + c_{v1}^3}, \quad X = \frac{\widetilde{v}}{v},$$

$$c_{b1} = 0.1355, \quad \sigma = \frac{2}{3}, \quad c_{b2} = 0.622\,, \quad \kappa = 0.41,$$

$$c_{w1} = \frac{{c_{b1}}^2}{\kappa} + \frac{1 + c_{b2}}{\sigma}, \quad c_{w2} = 0.3, \quad c_{w3} = 2, \quad c_{v1} = 0.1$$

2.4. Virtual Wind Tunnel Analysis and Boundary Conditions

The computational analysis consists of lattice structures shown in Figure 3. The dimensions of the numerical wind tunnel were selected as 3 m × 2 m× 6 m (width × height × length) to observe better analysis because it gives a suitable environment depending on turbine size, investigating the wake effect inside in virtual wind tunnel. Two cases were chosen to see the effect of several cells on the solutions: lattice structures with element numbers of about 2,500,000 and 5,000,000. In this simulation, an inlet wind velocity of 12 m/s is applied to predict the aerodynamic characteristics with various turbulence models in accordance with the reference [15]. An adaptive wake refinement technique observed detailed wake development around the blades. The XFlow engine incorporates an automatic scale adaptation feature that adjusts the resolved scales based on user-defined criteria. This adaptive process enhances the solution accuracy in regions near the walls by refining the mesh, effectively capturing strong gradients within the flow. Additionally, the engine dynamically adapts as the flow progresses to refine the wake region, ensuring an accurate representation of the evolving flow patterns. This behavior is illustrated in Figure 4, showcasing the adaptability and effectiveness of the XFlow engine in optimizing the solution quality throughout the computational domain.

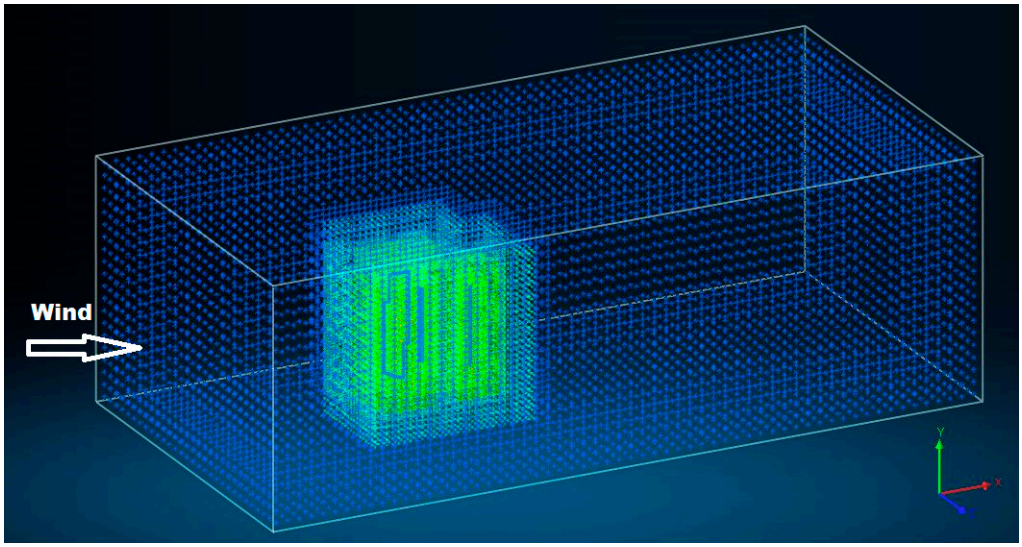

Figure 3. Cell Configuration of Darrieus Vertical Axis Wind Turbine (5,000,000 lattice cells).

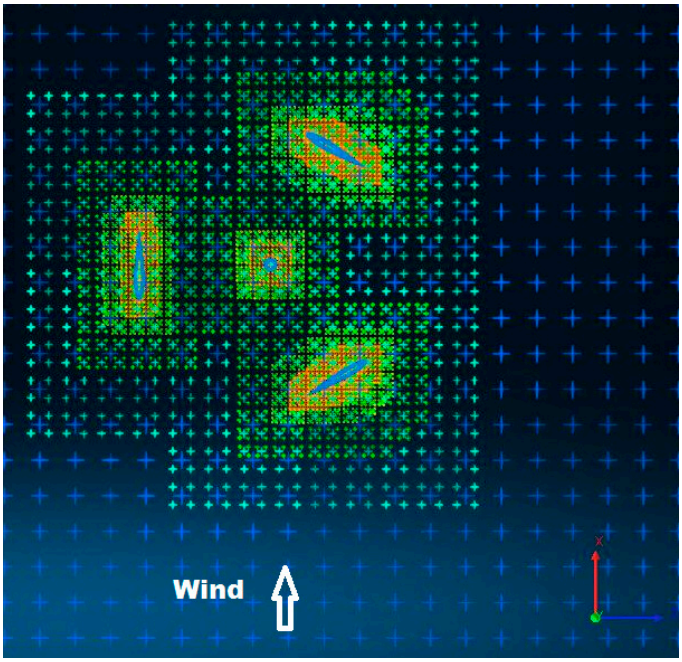

Figure 4. Adaptive Wake Refinement for Darrieus Vertical Axis Wind Turbine (5,000,0000 lattice cells). The spatial resolution varied from 0.00125 m to 0.05 m in this case. The wind direction using a white arrow, and we'll also represent the plane's orientation using a red arrow for the x-axis and a blue arrow for the z-axis.

The design parameters of the turbine and boundary conditions were specified according to the reference [15]. One of the performance parameters of wind turbines is the tip-speed ratio (TSR), which is the blade-tip speed against wind speed defined in Equation (10). Typically, the power performance of the rotor can be presented by variation of power coefficient with TSR. In a wind turbine, power obtains by multiplying the torque generated on the blades by the aerodynamic forces with the rotation speed. The torque coefficient (C_Q) and power coefficient (C_P) were calculated using Equations (11) and (12), respectively [15].

$$TSR = \frac{Tip\ Speed}{Wind\ Speed} = \frac{\omega \times R}{U_\infty} \tag{11}$$

$$C_Q = \frac{Q}{0.5\rho A R U_\infty} \tag{12}$$

In Equation (11), Q is torque [Nm], ρ denotes the air density [kg/m^3], and A is the cross-sectional area of the rotor [m^2] [15].

$$C_p = \frac{Q\omega}{0.5\rho A {U_\infty}^3} \tag{13}$$

To investigate the performance characteristics, three tip-speed ratios (TSRs) of 1, 1.2 and 1.6 were chosen for the calculations. Ref. [15] obtained the maximum power coefficient at TSR of 1.2 in their experimental results.

3. Results and Discussion

3.1. Solution Times with Different Turbulence Modelling Approaches

This study performed CFD solutions on an Intel® Xeon® CPU Process @3.50 GHz, 16 GB RAM, NVIDIA Quadro K4200 workstation operating on 12 CPUs. Mesh structures and their qualities may increase computational cost, and a higher-performance computer is required. However, LBM based on a particle-based approach uses a uniform Cartesian grid

that can be refined as it is required depending on geometry and flow field. To see the effect of the number of lattices on the solution time, the CPU times of solutions with different turbulence modelling approaches were given in Table 1.

Table 1. Overall CPU time (s) concerning several lattices in different turbulence models.

Number of Lattices	Overall CPU Time (s)		
	RANS Spalart Allmaras	**LES WALE**	**LES Smagorinsky**
2,500,000	1.13×10^4	1.16×10^4	1.18×10^4
5,000,000	1.64×10^4	1.77×10^4	1.87×10^5

The Courant Number plays a crucial role in governing the choice of time step scheme. By increasing the time step size, computational speed can be accelerated, making it desirable to set the Courant Number as high as feasible. On the other hand, smaller numbers mean a more stable solution but will be slower since it is doing more steps. The relation between the courant number and stable solution can be taken into consideration of the stability parameter. The stability parameter must be less than 1, so the configuration of the simulation time was adjusted to the given value of the Courant number of 0.8.

When the solution time displayed in Table 1 is compared, the RANS solution with the Spalart-Allmaras model had a lower computational time than the others for 2,500,000 and 5,000,000 lattices. Large-Eddy Simulation (LES) method, WALE and Smagorinsky turbulence models have greater values owing to the influence of time-dependent solution, as shown in Table 1. In other words, The RANS approach relies on ensemble-averaged equations, which limits its ability to predict local flow fluctuations. In contrast, the LES approach utilizes spatially filtered equations, allowing for capturing large-scale flow structures based on the chosen filter size.

3.2. Torque and Power Coefficients

Torque coefficients were obtained using the XFlow software by time averaging the instantaneous torque predictions. Results obtained with 2,500,000 lattices are displayed and compared with experimental data in Figure 5.

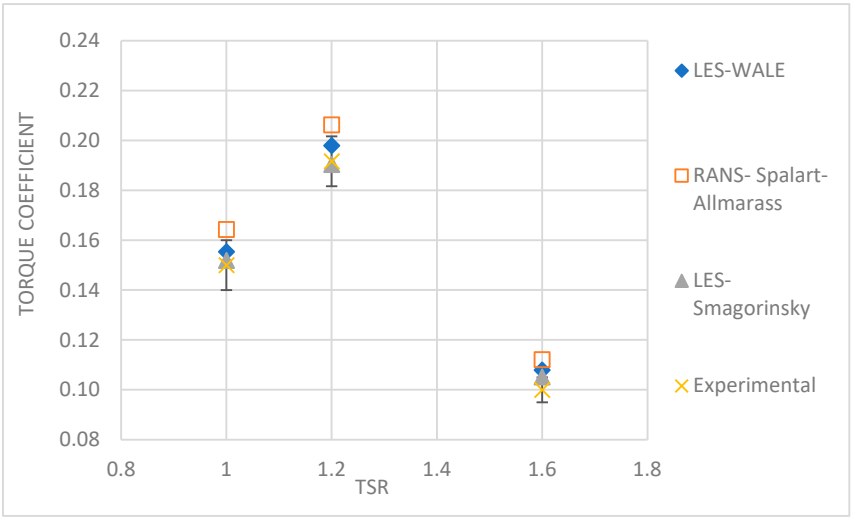

Figure 5. Variations in torque coefficients according to turbulence models and experimental results [15] for 2,500,000 lattices.

Figure 5 shows that the results do not all agree with the referenced experimental results. Here solutions with the Spalart-Allmaras model showed the worst agreement,

while the other predictions remained within the error bars of the measurements for TSRs of 1 and 1.2. Among the solutions, LES predictions with the Smagorinsky model yielded the best agreement.

To see the effect of several lattices on predictions, numerical solutions were repeated for a lattice size of 5,000,000. The corresponding torque coefficient predictions are displayed in Figure 6, along with the experimental data. The improvement in the predictions is evident from this figure, where all of them appeared inside the error bars of the measurement. Solutions obtained with the WALE method showed the best agreement with the experiment for this configuration.

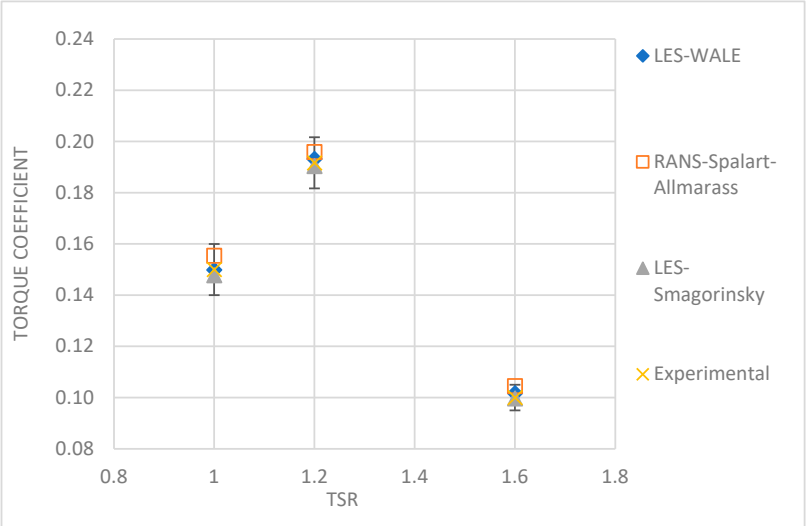

Figure 6. Variations in torque coefficients according to turbulence models and experimental results [15] for 5,000,000 lattices.

Overall, the agreement between the numerical predictions and experimental measurements was satisfactory for 5,000,000 lattices. Therefore, this lattice size was used in the rest of the study.

Figure 7 demonstrates the agreement between the WALE turbulence model and experimental results. Additionally, it can be observed that the power coefficient reaches a maximum at TSR 1.2 for 5,000,000 lattices.

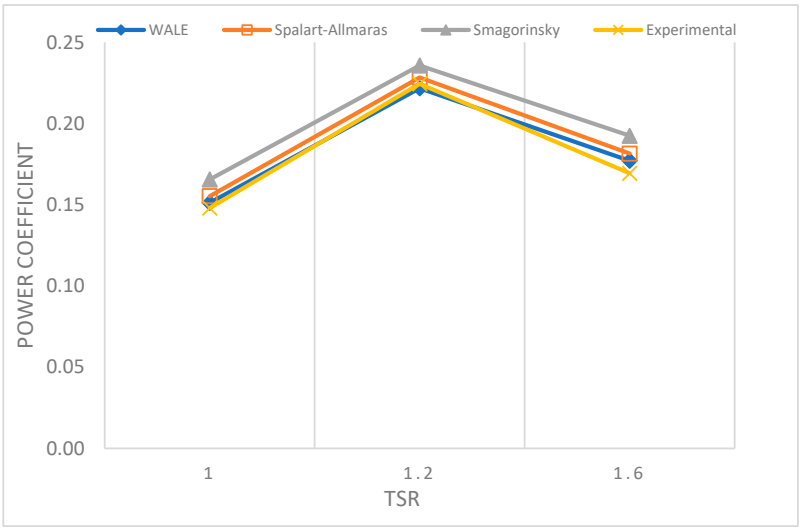

Figure 7. Variations in power coefficients according to turbulence models and experimental results [15] for 5,000,000 lattices.

3.3. Comparison of Flow Field Predictions with Different Turbulence Models

It is known that the structure of a VAWT causes more wake-blade interactions than a HAWT. Based on this idea, this study aimed to reveal the effect of different turbulence models on the wake predictions for a VAWT.

Contours distributions were taken from XFlow CFD software involving velocities and turbulence intensities at TSR1 and azimuthal angle, θ of 77°, as shown in Figures 8 and 9.

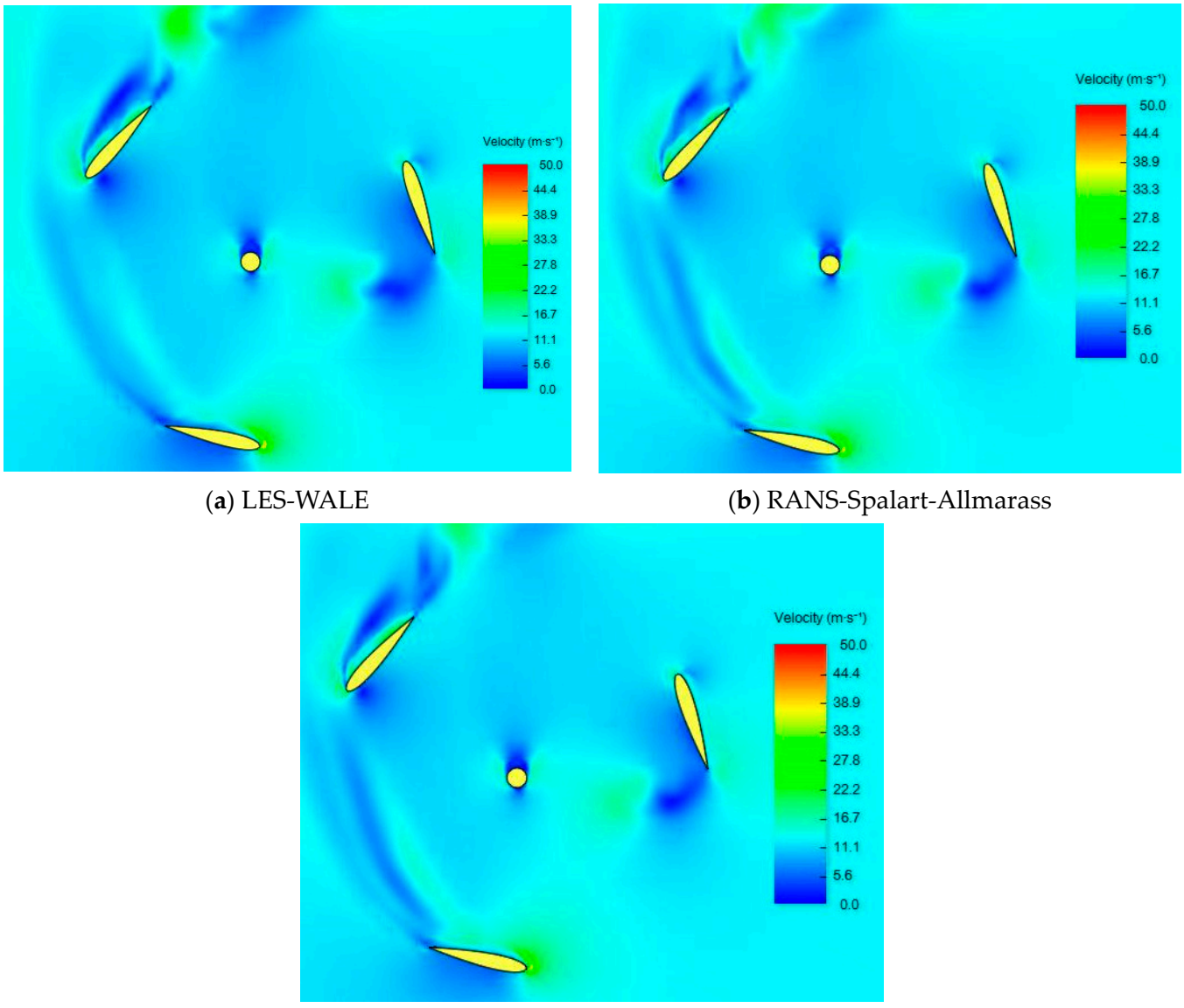

(**a**) LES-WALE (**b**) RANS-Spalart-Allmarass

(**c**) LES-Smagorinsky

Figure 8. Velocity contours around VAWT in different turbulence models for TSR 1 and θ = 77°.

The velocity distributions on the cutting plane are demonstrated in Figure 8. It shows that the boundary layer of the WALE and Spalart-Allmaras model gives a similar separation flow from the blade's surface. In contrast, the Smagorinsky turbulence model exhibits earlier flow separated from the blade surface. Figure 9 gives better results that enable us to understand changing viscosity effect on VAWT. Turbulence intensity provides to observe better wake predictions, the wake is separated from the trailing edge of the blade earlier, and LES-WALE model contours have a more intense wake structure than the other.

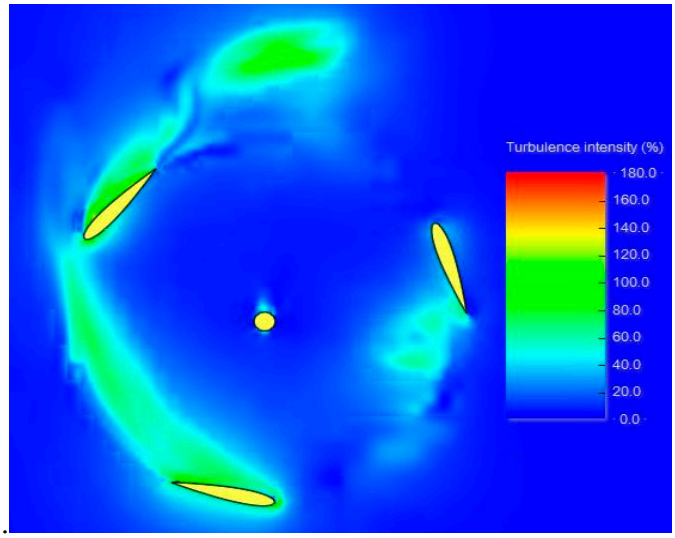

(**a**) LES-WALE

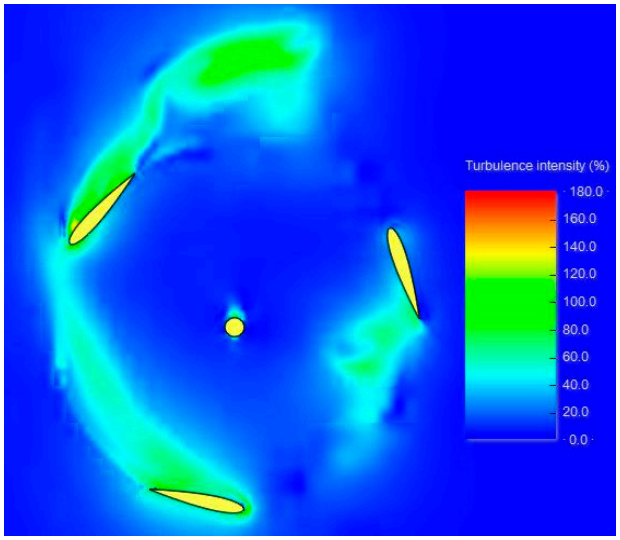

(**b**) RANS-Spalart-Allmaras

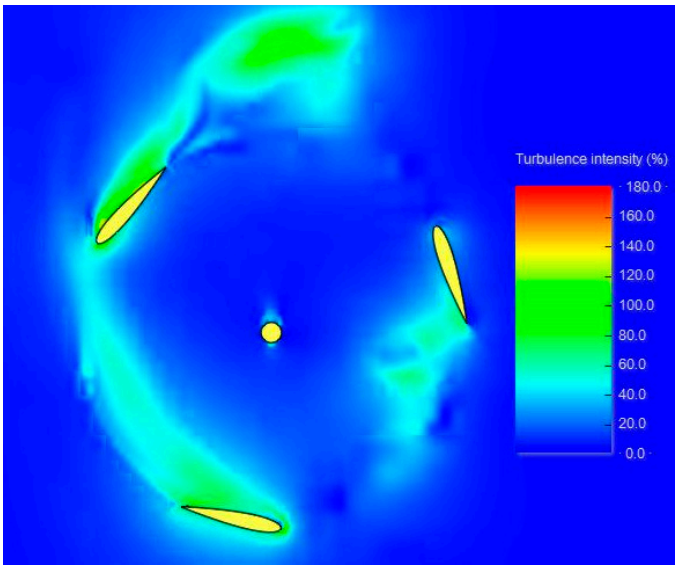

(**c**) LES-Smagorinsky

Figure 9. Turbulence Intensity (%) around VAWT in different turbulence models for TSR 1 and $\theta = 77^{\circ}$.

For TSR 1.2 and $\theta = 90^{\circ}$ velocities contours are found the higher values at RANS-Spalart-Allmaras turbulence model as shown in Figure 10. LES models show that WALE and Smagorinsky demonstrated more turbulence density around the blade, like each other, as shown in Figure 11.

As for TSR 1.6 and $\theta = 180^{\circ}$, RANS and LES modes reveal similar wake structures, and the higher rotor speed can be visualized to demonstrate wake predictions using vorticity structures. The RANS model, Spalart-Allmaras, agrees with the LES-WALE model at a higher rotor speed. LES-Smagorinsky showed that the wake is cutting from the flow separation of the trailing edge earlier, as shown in Figures 12 and 13.

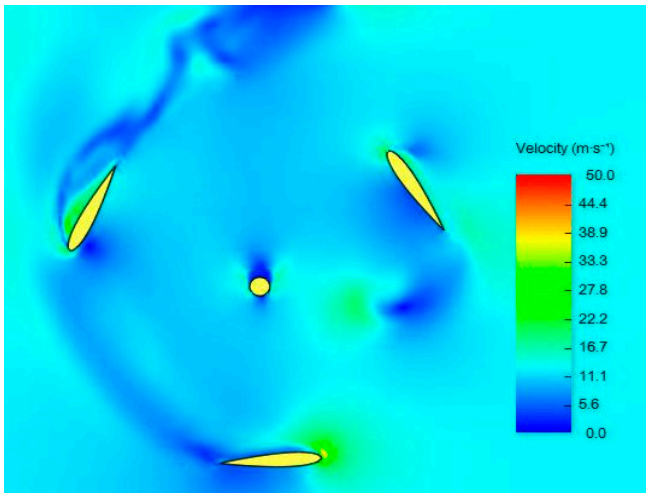

(**a**) LES-WALE

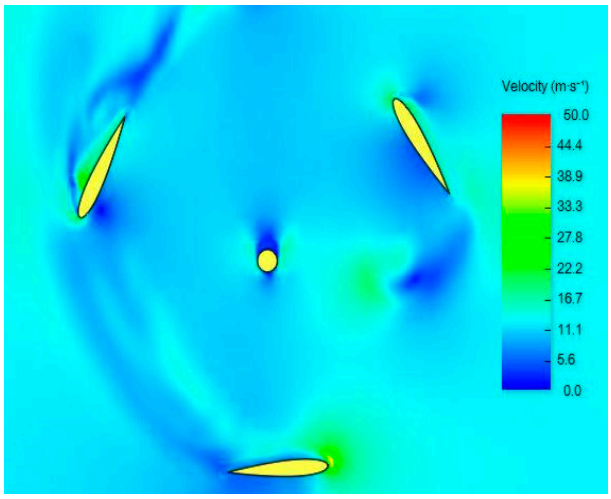

(**b**) RANS-Spalart-Allmaras

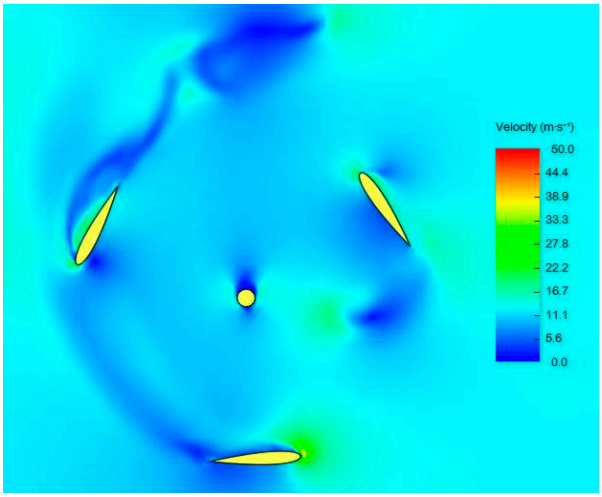

(**c**) LES-Smagorinsky

Figure 10. Velocity contours around VAWT in different turbulence models for TSR 1.2 and $\theta = 90°$.

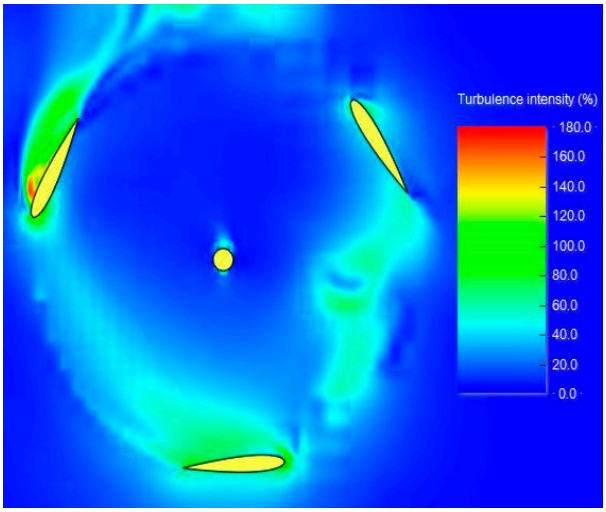

(**a**) **LES-WALE**

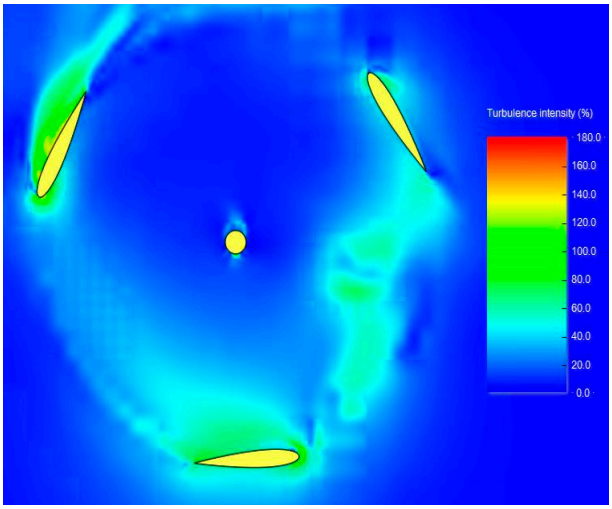

(**b**) **RANS-Spalart-Allmaras**

Figure 11. *Cont.*

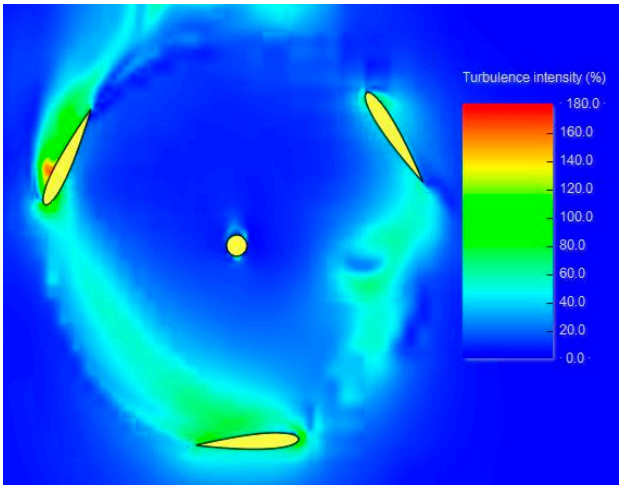

(c) LES-Smagorinsky

Figure 11. Turbulence Intensity (%) around VAWT in different turbulence models for TSR 1.2 and $\theta = 90°$.

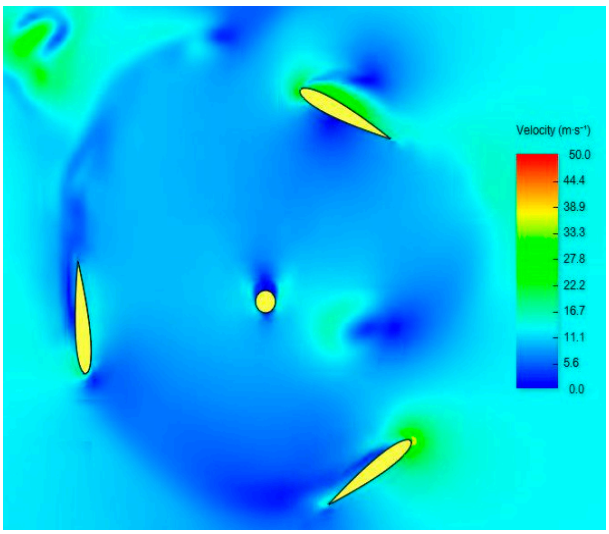

(a) LES-WALE

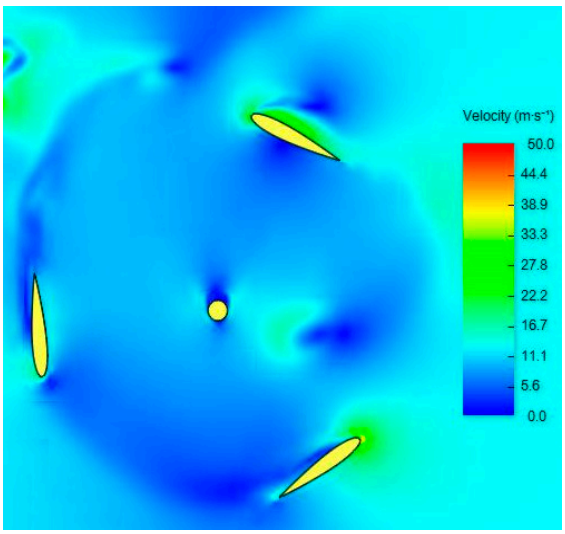

(b) RANS-Spalart-Allmaras

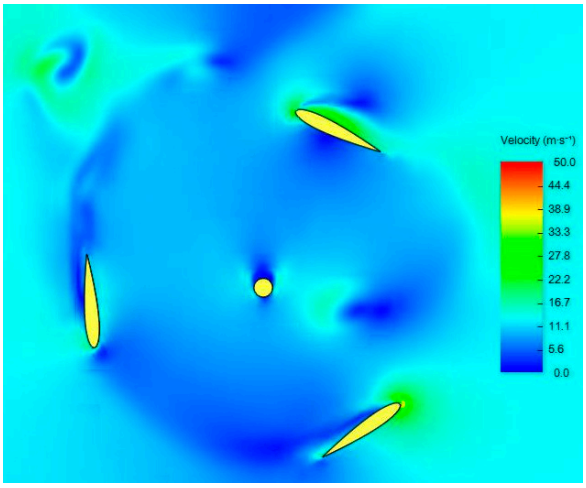

(c) LES-Smagorinsky

Figure 12. Velocity contours around VAWT in different turbulence models for TSR 1.6 and $\theta = 180°$.

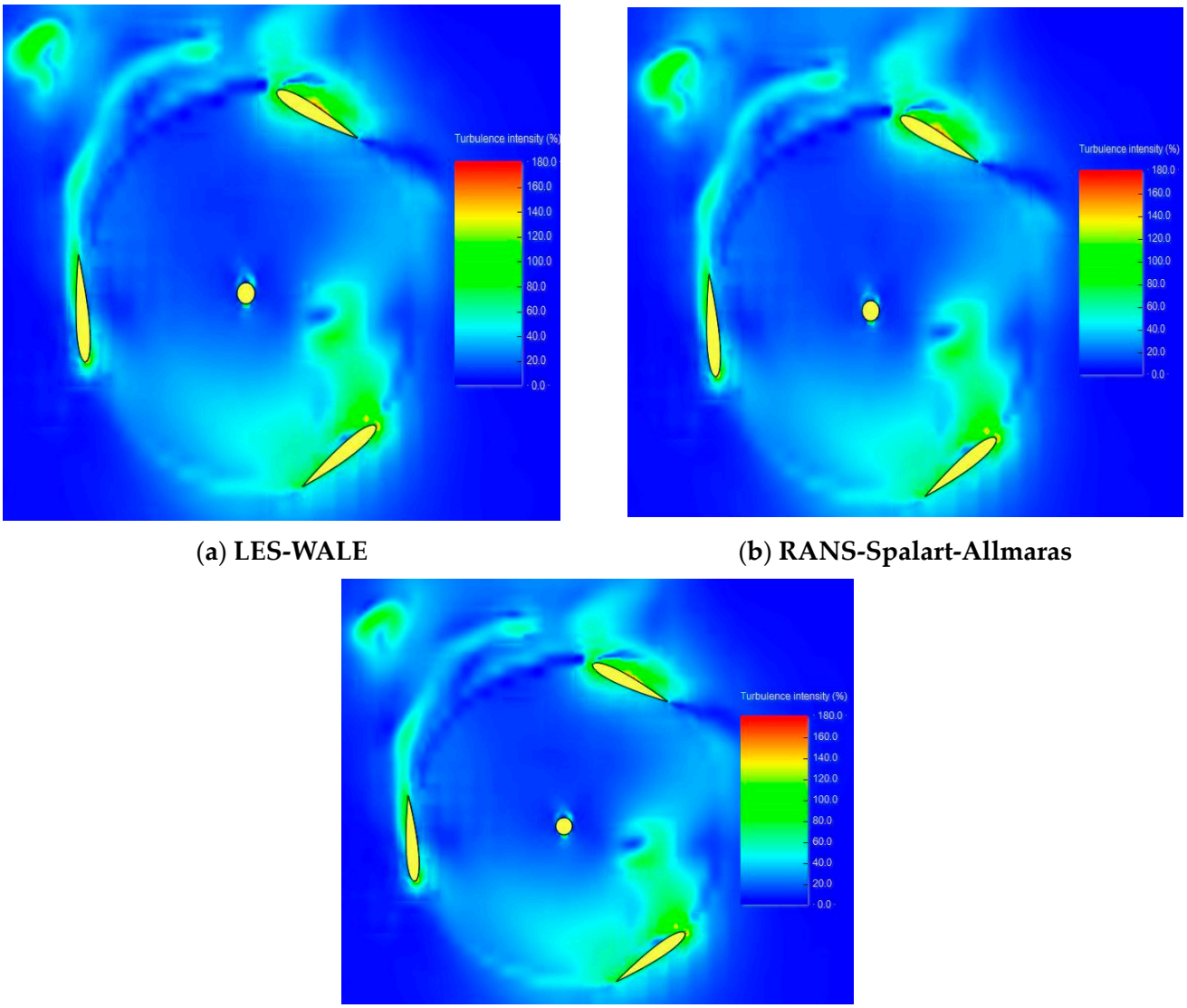

(**a**) **LES-WALE** (**b**) **RANS-Spalart-Allmaras**

(**c**) **LES-Smagorinsky**

Figure 13. Turbulence Intensity (%) around VAWT in different turbulence models for TSR 1.6 and $\theta = 180°$.

3.4. Investigation of Vorticity at Maximum Power Coefficient

At high angles of attack and low TSR, VAWTs undergo dynamic stalls, leading to complex flow structures around the blades. This phenomenon involves large, separated flow regions, vortex shedding, and potential blade vortex interactions. Despite the challenging aerodynamics, VAWTs can still generate power at low TSR due to these flow characteristics. Understanding and accurately modelling these flow phenomena are crucial for optimizing VAWT design and performance under dynamic stall conditions.

Vorticity behind the blades and turbine is a significant factor, performing at maximum power and torque coefficient, to enable the examination of the influence of different turbulence models. As seen in Figures 14–16, the vorticity measurements while the wind passes around the turbine and blades raise the value of vorticity around the blade as it rotates and entry to the path of the other blade flowing in the wind tunnel.

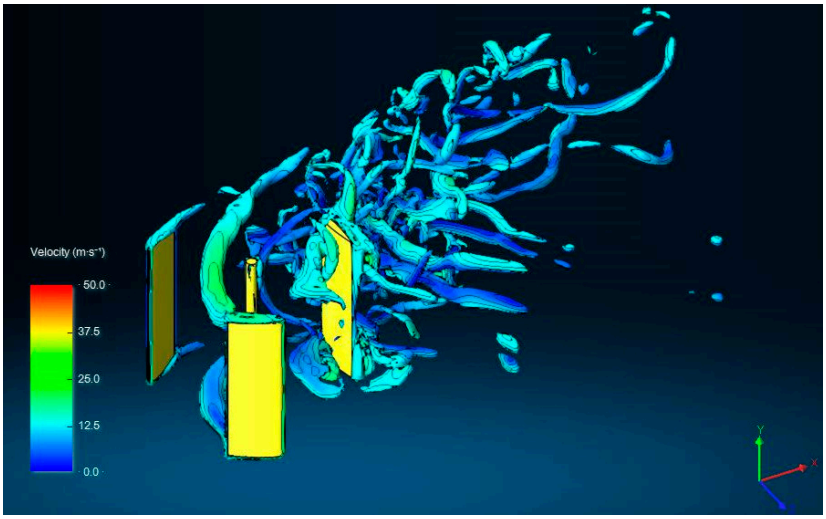

Figure 14. Vorticity coloured by field Velocity for LES-WALE turbulence model for TSR 1.2.

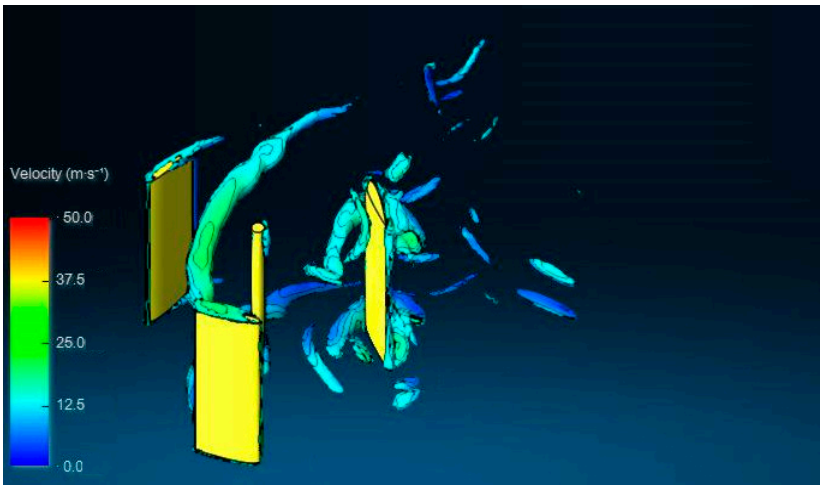

Figure 15. Vorticity coloured by field Velocity for RANS-Spalart-Allmaras turbulence models for TSR 1.2.

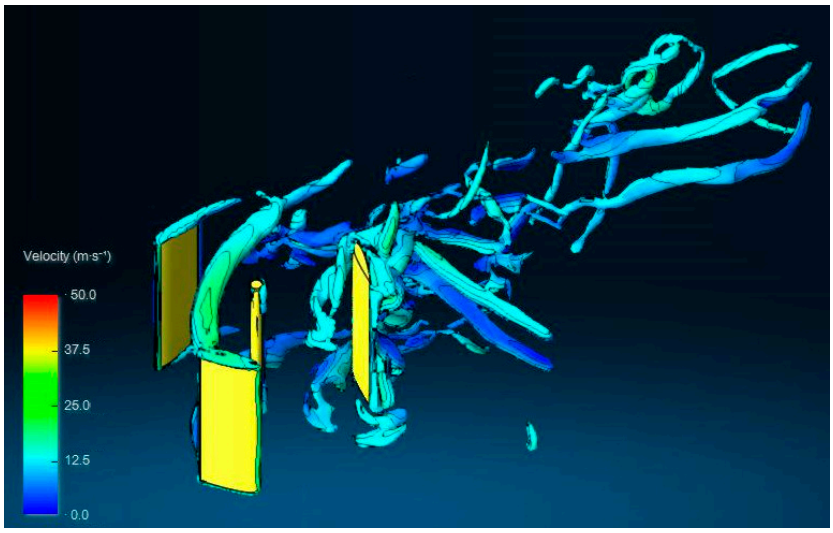

Figure 16. Vorticity coloured by field Velocity for LES-Smagorinsky turbulence models for TSR 1.2.

One of the basic schemes, vorticity coloured by field velocity, was used to observe the wake structures in the flow field. It is beneficial when compared with RANS, LES turbulence models reveal existing wake structures and velocities behind the VAWT. Furthermore, LES models, WALE and Smagoringsky, demonstrate individually the different wake structures even if they are in the same class. The visualization in Figures 14–16 depicts the turbulent structures, showcasing distinct vortex shapes formed behind the rotating blades under varying turbulence models (WALE, Smagorinsky, Spalart-Allmaras). These figures provide insights into the characteristic features of the vortices when the wind originates from the left side. In the figures, when the TSR is 1.2, the WALE turbulence model shows long vorticity intensity compared to the RANS-Spalart Allmarass and Smagorinsky turbulence models. Thus, it was clear that LES WALE turbulence models enable us to observe the wake predictions behind the VAWT.

4. Conclusions

This work investigated Darieus-type 500 W straight-bladed Vertical axis wind turbine (VAWT) using XFlow commercial software, using a meshingless Lattice Boltzmann method for different turbulence models in fine and coarse lattices.

To assess the validity of the proposed numerical modelling, offering the meshingless lattice Boltzmann method, which users can avoid the remeshing process for CFD simulation, enables the investigation of the aerodynamic performance of wind turbines with fewer lattices, saving time and computational costs.

Firstly, the influence of different turbulence modelling approaches on solution time was investigated depending on lattice sizes. It appeared that the RANS model could give a faster solution than the LES approaches even when the number of lattices is increased. The increase in the number of lattices is not changing the solution time proportionally.

Secondly, experimental data on torque coefficient obtained from [15] were compared with different turbulence models in fine and coarse lattices. LES models, WALE and Smagorinsky, demonstrated the best agreement with experimental data. Especially, Smagorinsky model can be useful when less computational cost is required, and WALE is a suitable turbulence model that best agrees with experimental data to capture the maximum torque and power coefficient as users analyse the VAWT at the fine lattices.

The effect of turbulence models is achieved by the velocity and turbulence intensity contours at different TSR values. RANS and LES models give an observable wake structure behind the rotating blades, especially at maximum torque coefficient. However, the LES model is useful when compared to the result with experimental in fine lattices.

The result is also given by investigating vorticity at maximum power coefficient at varying azimuthal angles. LES models exhibit considerable differences in the wake predictions when compared with RANS. LES-WALE model has more intense wake structures, it is the reasonable effect of the LES model constant and its operator based on the formula, including the rotation tensor.

In addition, a comprehensive sensitivity analysis has been conducted to investigate the behaviour of VAWTs further. Surprisingly, the study reveals that capturing the flow phenomenon does not require an excessively fine grid, despite the significant flow separation observed. The simulation results are compared with both numerical and experimental data, and although some discrepancies exist, they are relatively minor when using fine lattices.

Moreover, the study highlights an interesting finding: the power performance of the VAWT increases as the TSR rises, particularly at low TSRs. However, at high TSRs, the interaction between vortices and blades becomes more prominent and significantly influences the blade's performance.

Author Contributions: Writing—original draft preparation, C.L.; supervision, E.A. All authors have read and agreed to the published version of the manuscript.

Funding: This work was supported by the Scientific Research Projects Commission (BAPKO) of Marmara University under grant number FEN-C-DRP-130515-0179.

Institutional Review Board Statement: The study did not require ethical approval.

Informed Consent Statement: The study did not involve humans.

Data Availability Statement: The benchmark data is available at Lee, Y.; Lim, H. Numerical study of the aerodynamic performance of a 500 W Darrieus-type vertical-axis wind turbine. Renew. Energy 2015, 83, 407–415.

Conflicts of Interest: The authors declare no conflict of interest.

References

1. Islam, M.; Fartaj, A.; Carriveau, R. Analysis of the design parameters related to a fixed-pitch straight-bladed vertical axis wind turbine. *Wind Eng.* **2008**, *32*, 491–507. [CrossRef]
2. Elkhoury, M.; Kiwata, T.; Aoun, E. Experimental and numerical investigation of a three-dimensional vertical-axis wind turbine with variable-pitch. *J. Wind Eng. Ind. Aerodyn.* **2015**, *139*, 111–123. [CrossRef]
3. Howell, R.; Qin, N.; Edwards, J.; Durrani, N. Wind tunnel and numerical study of a small vertical axis wind turbine. *Renew. Energy* **2010**, *35*, 412–422. [CrossRef]
4. Zhang, L.; Luo, K.H.; Lu, X. Lattice Boltzmann simulation of convective heat transfer enhancement with microencapsulated phase change material in thermal energy storage systems. *Int. J. Heat Mass Transf.* **2023**, *172*, 121104.
5. Chen, L.; Huang, H.; Li, X. Microscale gas flow simulation using the lattice Boltzmann method with thermal creep boundary conditions. *Phys. Rev. E* **2022**, *102*, 013306.
6. Musavi, S.M.; Ashrafizaadeh, M. A mesh-free lattice Boltzmann solver for flows in complex geometries. *Int. J. Heat Fluid Flow* **2016**, *59*, 10–19. [CrossRef]
7. Li, S.; Zheng, Y.; Zhang, X.; Luo, K.H. Large-scale lattice Boltzmann simulations of turbulent channel flows on a GPU cluster. *Int. J. Heat Mass Transf.* **2022**, *157*, 119874.
8. Wang, Y.; Zhou, H.; Zhang, X. Large-scale lattice Boltzmann simulation of transitional channel flows on GPU clusters. *Int. J. Heat Mass Transf.* **2023**, *170*, 120693.
9. Liu, Y.; Wang, Y.; Zhang, H.; Zhang, Y. Lattice Boltzmann simulation of two-dimensional heat transfer in porous media with solid matrix heterogeneity. *Int. J. Heat Mass Transf.* **2022**, *157*, 119876.
10. Park, J.W. Application of mesh free lattice Boltzmann method to the analysis of very high temperature reactor lower plenum. *Atw. Int. Z. Kernenerg.* **2011**, *56*, 636–640.
11. Holman, D.M.; Brionnaud, R.M.; Abiza, Z. Solution to industry benchmark problems with the lattice-Boltzmann code XFlow. In Proceedings of the European Congress on Computational Methods in Applied Sciences and Engineering (ECCOMAS 2012), Vienna, Austria, 10–14 September 2012.
12. Wood, S.L.; Deiterding, R. A Lattice Boltzmann Method for Horizontal Axis Wind Turbine Simulation. In Proceedings of the 14th International Conference on Wind Engineering, Porto Alegre, Brazil, 21–26 June 2015.
13. Safdari, A.; Kim, K.C. Aerodynamic and Structural Evaluation of Horizontal Archimedes Spiral Wind Turbine. *J. Clean Energy Technol.* **2015**, *3*, 34–38. [CrossRef]
14. Amine, B.A.M.E.; Chekib, K.; Sassi, B.N. Computational Fluid Dynamics study of Vertical Axis Wind Turbines in different shapes. In Proceedings of the VI ème Congrès International sur les Energies Renouvelables et l'Environnement, Hammamet, Tunisie, 19–21 March 2012.
15. Lee, Y.; Lim, H. Numerical study of the aerodynamic performance of a 500 W Darrieus-type vertical-axis wind turbine. *Renew. Energy* **2015**, *83*, 407–415. [CrossRef]
16. Qian, Y.H.; d'Humieres, D.; Lallemand, P. Lattice BGK models for Navier-Stokes equation. *Europhys. Lett.* **1992**, *17*, 479. [CrossRef]
17. Zhuo, C.S.; Zhong, C.W. LES-based filter-matrix lattice Boltzmann model for simulating turbulent natural convection in a square cavity. *Int. J. Heat Fluid Flow* **2013**, *42*, 10–22. [CrossRef]
18. Weickert, M.; Teike, G.; Schmidt, O.; Sommerfeld, M. Investigation of the LES WALE turbulence model within the lattice Boltzmann framework. *Comput. Math. Appl.* **2010**, *59*, 2200–2214. [CrossRef]
19. Krafczyk, M.; Tölke, J.; Luo, L.S. Large eddy simulations with a multiple-relaxation-time LBE model. *Int. J. Mod. Phys. B* **2003**, *17*, 33–39. [CrossRef]
20. Huang, C.; Zhou, P.; Meng, J. Lattice Boltzmann modeling of gas–liquid two-phase flow in porous media. *J. Pet. Sci. Eng.* **2022**, *195*, 107978.
21. Tang, Y.; Zhang, Z.; Luo, K.H. Multiphase lattice Boltzmann simulations of boiling heat transfer: Influence of substrate wettability. *Int. J. Heat Mass Transf.* **2023**, *152*, 119550.